A new empirical model to estimate hourly diffuse photosynthetic photon flux density

I. Foyo-Moreno, (1,2), I. Alados (3,2) and L. Alados-Arboledas (1,2)

(2) Andalusian Institute for Earth System Research (IISTA-CEAMA), 18006 Granada, Spain

(3) Dpto de Física Aplicada II, Universidad de Málaga, Málaga, Spain.

Corresponding author:

I. Foyo-Moreno

Departamento de Física Aplicada

Facultad de Ciencias

Universidad de Granada

18071, Granada

Spain.

Phone: 34 58 240022

FAX: 34 58 243214

E-mail: ifoyo@ugr.es

ABSTRACT

Knowledge of the photosynthetic photon flux density (Q_p) is critical in different applications dealing with climate change, plant physiology, biomass production, and natural illumination in greenhouses. This is particularly true regarding its diffuse component (Q_{pd}), which can enhance canopy light-use efficiency and thereby boost carbon uptake. Therefore, diffuse photosynthetic photon flux density is a key driving factor of ecosystem-productivity models. In this work, we propose a model to estimate this component, using a previous model to calculate Q_p and furthermore divide it into its components. We have used measurements in urban Granada (southern Spain), of global solar radiation (R_s) to study relationships between the ratio Q_{pd}/R_s with different parameters accounting for solar position, water-vapour absorption and sky conditions. The model performance has been validated with experimental measurements from sites having varied climatic conditions. The model provides acceptable results, with the mean bias error and root mean square error varying between -0.3 and -8.8% and between 9.6 and 20.4%, respectively.

1. INTRODUCTION

The amount of photosynthetically active radiation (PAR), defined as the visible portion of global solar radiation (R_s) used in photosynthesis to convert light energy into biomass (Udo and Aro, 1999; Jacovides et al., 2004; Tang et al., 2013), determines the exchanges of energy and water between the land surface and the atmosphere. Among the standard environmental statistics needed to evaluate plant photosynthesis are PAR data

(Akitsu et al., 2017). This radiation covering both photon and energy terms lies between 400 and 700 nm. Thus, the photosynthetic photon flux density, Q_p, is defined as the photon flux density (1 µmol photons m^{-2} s^{-1}=6.022*10^{17} photons m^{-2} s^{-1}). This is the number of photons in the 400-700 nm waveband incident per unit time on a unit surface.

The amount and spectral quality of the radiation reaching the surface is altered by aerosols and clouds by absorption and scattering processes, varying the proportion of the components of radiation (direct and diffuse). Plants use both the direct and diffuse photosynthetic photon flux density (Q_{pb} and Q_{pd}), but it is known that these components differ in the way they transfer energy through plant canopies and affect the summation of nonlinear processes such as photosynthesis differently than would occur at the leaf scale (Gu et al., 2002; Misson et al., 2005; Min, 2005; Jacovides et al., 2007; 2010). In fact, the efficiency with which incoming PAR is intercepted by a canopy, depends on its efficiency in intercepting direct and diffuse incoming radiation and on the proportions of Q_{pd} and Q_{pb} (Alados et al., 2002).

The analysis of the effects of Q_{pd} on ecosystem productivity has become one of the main goals in terrestrial carbon-cycle research (Gu *et al.*, 1999, 2002, 2003; Mercado *et al.*, 2009; Sun and Zhou, 2010; Zhang *et al.*, 2010; He *et al.*, 2011; Zhang *et al.*, 2011), and thus the treatment of Q_{pd} in ecosystem models is needed (Gu *et al.*, 2003; Mercado *et al.*, 2009; Kanniah *et al.*, 2012). Hence, quantifying Q_{pd} and understanding its spatiotemporal variations are critical for estimating its impact on the carbon cycle of terrestrial ecosystems. Currently, many sites measure Q_p, although a worldwide network for routinely measuring Q_p has not yet been established, despite the biological importance of this radiometric quantity. Furthermore, few observation sites measure Q_{pd}, raising the need for models to estimate these data. Q_{pd} is usually estimated by multiplying Q_p by the diffuse fraction of global radiation (k_d=R_d/R_s), where R_d is diffuse irradiance, but this is only a rough estimate because k_d is not equivalent to the diffuse fraction in the visible range (k_{dQp}), which is significantly greater than k_d under clear skies, although almost equivalent under cloudy skies (Spitters *et al.*, 1986).

In the present work, we have evaluated a model to estimate Q_{pd} using a previous model to estimate Q_p (Foyo-Moreno et al., 2017), considering the separation of R_s into its components: direct and diffuse. Prior to evaluating model performance, we have analysed dependences of the Q_{pd}/R_d ratio and Q_{pd} on different parameters. These parameters describe the solar position using the cosine of the solar zenith angle (θ) and indices such as sky clearness ($\varepsilon = (R_d + R_b)/R_d$), sky brightness ($\Delta = R_d/R_{so}\cos\theta$), and the clearness index ($k_t = R_s/R_{so}$), where R_d is diffuse irradiance, R_b is direct normal irradiance and R_{so} is the extraterrestrial global solar irradiance (Pérez et al., 1990; Alados et al., 1996). For example, Jacovides et al. (2007; 2010) proposed an empirical model relating k_{dQp} to the clearness index Q_p ($k_{tQp} = Q_p/Q_{po}$), where Q_{po} is the extraterrestrial photosynthetic photon flux density. To consider the effects of water absorption in this spectral range, we also analysed dependence on meteorological parameters such as water-vapour pressure (e) or dew-point temperature (T_d). The model proposed in this work uses as input data the solar position as the cosine function of the solar zenith angle (□) and diffuse irradiance (R_d). The model was evaluated with a set of independent data at various sites, two in Spain and another in Italy, with different climatological characteristics.

2. EXPERIMENTAL SITE AND MEASUREMENTS

In this work, we used data from three sites (Granada and Almería in Spain, and Renon in Italy). The data from Granada were used to study the main dependence between the variables of interest for this study, and all three stations were used to validate the proposed model, since this proposal is based on a previous model to estimate Q_p (Foyo-Moreno et al., 2017), with data compiled for Granada during other years vs. those used in the present work. Ground-based data for two years at 1-min intervals were acquired at a station on the outskirts of Granada (37.18° N, 3.58° W, 660 m a.s.l.). From this data base, hourly values were generated for the entire two-year period to include a wide range of seasonal conditions and solar zenith angles. The photosynthetic active photon-flux density (Q_p) was measured using LICOR model 190 SA quantum sensors (Lincoln, Nebraska, USA). Another quantum sensor has been equipped with a polar axis shadowband to measure the diffuse photosynthetic active photon flux density (Q_{pd}). Global solar irradiance, R_s, was measured using a Kipp and Zonen model CM-11 radiometer (Delft, Netherlands), while another CM-11 with a polar axis shadowband was used to measure diffuse solar irradiance (R_d). The diffuse-irradiance measurements were corrected following the method proposed by Batlles et al. (1995). The quantum sensor has a relative error of less than 5% relative to the values measured, and global solar-irradiance measurements have an estimated experimental error of about 2-3%. The calibration constants of the instruments were periodically checked (Alados and Alados Arboledas, 1999).

To avoid problems associated with instrument deviations from the ideal cosine law, we limited our study to solar zenith angles of less than 85º (Alados et al., 1996). We evaluated the proposed model using data from different stations that had not been used in building the model, two in Spain (Granada and Almería), and another in Italy (Renon). Detailed information on the instrumentation and site characteristics can be found for Almería in Alados and Alados-Arboledas (1999). The radiometric sensors used at Almería are similar to those used at Granada. The Renon/Ritten site (Italy), is operated by the Forest Service and the Agency of the Environment of the Autonomous Province of Bolzano (APB). In Italy, Q_p was measured by a BF2 sunshine sensor (Delta-T Devices, Burwell, Cambridge, United Kingdom). This device uses an array of silicon photodiodes and a shading pattern on the radiometer dome to determine Q_{pd}. The accuracy of these sensors is 15% (BF2, Delta-T Devices, 2005).

Table 1 presents some climatic data for the stations used. Granada is an inland location in south-eastern Spain, a non-industrialized medium-sized city situated in a natural basin surrounded by mountains with elevations between 1000 and 3500 m a.s.l.. Near continental conditions prevailing at this site are responsible for large seasonal temperature differences, providing cold winters and hot summers. Most rainfall occurs during winter and spring. Almería, located on the Mediterranean coast in south-eastern Spain, has frequent cloudless days and high humidity. Renon is situated at 1735m a.s.l. in the Italian Alps in Bolzano (Alto Adige, Italy). This site is influenced by an windy and humid alpine climate. Thus, the three sites present contrasting climatic characteristics and altitudes. The yearly precipitation markedly fluctuates.

3. RESULTS AND DISCUSSION

3.1. ANALYSIS OF Q_{pd}/ R_d RATIO

As in our earlier work (Foyo-Moreno et al., 2017), before the direct study of the variable of interest (Q_{pd}), we analysed the ratio between Q_{pd} and R_d (Q_{pd}/R_d) with different parameters. Other works (Alados et al. 1996, Yu et al. 2015, Yu and Go, 2016) showed seasonal and daily variations of Q_p/R_s and also variations of Q_{pd}/R_d (Alados and Alados-

Arboledas, 1999). Since the most important factor influencing the solar-radiation levels reaching the Earth's surface is solar position, Figure 1 shows this dependence of this ratio on cosθ. We noted that this ratio varied between 1.86 and 2.48 μmol J^{-1} with a mean value of 2.19 ± 0.13 (μmol J^{-1}). Jacovides et al. (2007) found a mean value in Athens (Greece) of 2.43 ± 0.26 (μmol J^{-1}). For all hourly values together, we found no dependence. However, for the mean values of this ratio in different categories of cosθ, we detected a slight dependence with high dispersion. The correlation coefficient (R^2) was 0.54 while the intercept and slope were 2.14 ± 0.02 (μmol J^{-1}) and 0.08 ± 0.02 (μmol J^{-1}), respectively. The positive dependence with cos θ implies a reduction in the relative contribution of photosynthetically active photon flux density over the whole solar spectrum when the optical air mass increases. In Almería (Spain) a similar dependence has been reported (Alados et al., 1999). In an initial approximation, we could assume that this ratio was constant and we calculated Q_{pd} from R_d.

The second dependence analysed was on R_s (Figure 2) and the third on R_d (Figure 3). There was no dependence on R_s for all hourly values but a positive correlation was found for the mean values considering the categories with the R_s values. However, a clearer dependence for all hourly values was detected, although with great dispersion, as a function of R_d, with larger values for low values of R_d. Thus, with decreasing R_d (clear skies), the diffuse component of Q_p was larger than the diffuse component for R_d.

In our search for a more direct relation with sky condition, Figure 4 shows the dependence of this ratio on the clearness index (k_t). This parameter is defined as the ratio of the global irradiance (R_s) to the extraterrestrial global irradiance (R_{so}), both on a horizontal surface:

$$k_t = \frac{R_s}{R_{so}} \qquad (1)$$

with $R_{so} = E_o I_{sc} \cos\theta$. E_o is the eccentricity correction factor and the value used of the solar constant (I_{sc}) is 1367 Wm^{-2} (Iqbal, 1983). Details of the calculation of $\cos\theta$ can be found by Iqbal (1983). The parameter k_t characterizes the sky condition including the attenuation effects of the most dominant factors controlling solar radiation, such as clouds and aerosols. Previous studies used similar parameters such as the sky clearness and the skylight brightness (Pérez et al., 1990) to characterize the sky condition (Alados et al., 1996). Another parameter to characterize sky condition is diffuse fraction (k_d), defined as the ratio between diffuse global irradiance (R_d) and global irradiance (R_s):

$$k_d = \frac{R_d}{R_s} \qquad (2)$$

Knowledge of k_d can be useful to get an idea of atmospheric load indirectly, where a low k_d indicates a clear sky and more pristine atmosphere, while high k_d values denote high aerosol loads (Singh et al., 2013). In fact, the ratio between R_d and R_{bn} can be used to estimate aerosol optical depth (Foyo-Moreno et al., 2014).

Figures 4 and 5 show the dependence of Q_{pd}/R_d on these parameters. There is a slight dependence on k_t for all hourly data and for mean values in categories of k_t values, higher values of the Q_{pd}/R_d ratio are detected for low and high k_t values. These high values of Q_{pd}/R_d for high values of k_t are consistent with Jacovides et al. (2007), who reported a weak correlation for daily values, which is well fit by an exponential equation with a determination coefficient of 0.276. They found hourly ratio values varying from 2.56 ± 0.27 to 2.42 ± 0.24 (µmol J^{-1}), and ratios under clear skies 5.5% higher than that for overcast skies. These results agree with Alados and Alados-Arboledas (1999) and Min (2005). In any case, high k_t values imply low k_d values, so that this ratio had high values for low values of k_d (clear skies) although the dispersion of data was high (Figure 5), increasing the dispersion with k_d. Under clear skies, the regulating factors in the solar radiation modification are scattering processes, so that spectral investigations support the premise that, under these skies with aerosol loads, short wavelengths are preferentially scattered, thus increasing Q_{pd} more than R_d (Jacovides et al., 2000; Dye, 2004). However, the pattern observed for low values of k_t (<0.4) is different (Figure 4), the ratio decreasing when k_t increases. This result could be associated with the mixed effects of aerosols and clouds, because these cases correspond to skies with high opacity.

From the above analysis, it is clear that this ratio varies with changing sky conditions. Clouds exhibit relatively constant extinction across the visible spectrum while aerosols commonly show extinction that significantly diminishes the greater the wavelength (Min, 2005; Jacovides et al., 2007). This result can be attributed to the presence of clouds in skies with the high solar absorption in the infrared region (NIR). Clouds absorb NIR more strongly than Q_p, and hence the transmittance of Q_p through clouds is larger than NIR. In fact, clouds more markedly attenuate the total solar spectral range than they do shorter wavelengths such as the ultraviolet range (Foyo-Moreno et al., 2001, 2003).

As in an earlier work (Foyo-Moreno et al., 2017), here, to explicitly consider absorption by water vapour in the solar spectrum, we have shown in Figures 6 and 7 the dependence on meteorological parameters such as the dewpoint temperature (T_d) – relevant due to its correlation with precipitable water (Reitan, 1963) – and the partial vapour pressure (e). T_d and e have been calculated from the direct measurements of air temperature (T) and the relative humidity (U) at our station, with standard formulation. As before

(Foyo-Moreno et al., 2017), no dependence was detected.

3.2. ANALYSIS OF PARAMETERS CHARACTERIZING SKY CONDITIONS

Now, in order to find relationships between parameters considering sky conditions, it is possible to define indexes for the visible range equivalent to those for the shortwave broadband range. These parameters are $k_{tQp} = Q_p/Q_{po}$ (clearness index) and $k_{dQp} = Q_{pd}/Q_p$ (diffuse fraction), defined as in Eqs. 1 and 2, respectively but for the visible range. Q_{po} can be derived from R_{so}, with a fraction of 0.5 suggested by most studies (Frouin and Pinker 1995; Hu et al. 2007, 2010; Wang et al. 2014), then Q_{po} can be calculated by multiplying by the ratio 4.57 of the energy-flux density to photosynthetic photon flux density (Dye 2004). Figure 8 shows the dependence between k_{dQp} and k_{tQp}. Jacovides et al. (2007) found a polynomial fitting, shown in Figure 8 as the dashed line for $0.1<k_{tQp}<0.85$. Our fitting is also a third-order polynomial but with different coefficients (solid line) with a determination coefficient of 0.88. For low values of k_{tQp} the diffuse component is similar to Q_p and for high values this proportion decreases to about 10% of Q_p. In the literature, few studies have focused on the empirical relationships between Q_p and Q_{pd} of the Liu and Jordan regression type (Jacovides et al., 2010). The applicability of several diffuse radiation empirical models has been analysed in Athens (Jacovides et al., 2010), showing mean bias error (MBE) values between -12.9 and 2.99 % and root mean square error (RMSE) values between 27.1 and 35.6%, with a MBE of 0.11% and a RMSE of 26.8% for their fitting.

Figure 9 shows the dependence between the ratio of the diffuse fraction in the visible range (k_{dQp}) and the diffuse fraction in the shortwave broadband range (k_d) and clearness index (k_t). We found a positive correlation, with the ratio increasing with clear skies. Spitters et al. (1986) showed that the diffuse fraction for the visible range was 1.4 times the diffuse broadband fraction under clear sky conditions. It is evident that this ratio increases significantly when sky conditions change from cloudy to clear. In our case, the value found was 1.17 ± 0.07 for clear skies. Jacovides et al. (2007) reported a value of 1.38 ± 0.32. The dispersion increases with higher k_t values. However, for low values of k_t (<0.4; cloudy skies) the diffuse fraction in the visible range is of the same order as the diffuse fraction in the shortwave broadband range.

3.3. ANALYSIS OF Q_{pd}.

In this section, we directly study the dependence of Q_{pd} on the same parameters considered in Section 3.1. First, we show that the solar zenith angle alone does not allow for a correct determination of Q_{pd} (Figure 10). While Q_{pd} increases with decreasing θ, due to high dispersion it is possible to parameterise only the two *envelopes* of the data through a simple linear dependence on the cosine of θ. This result is similar to earlier work with Q_p (Foyo Moreno et al., 2017), and with the ultraviolet range (Foyo-Moreno et al., 1998, 2007). The upper envelope of the data corresponds to the maximum values that can be assumed to correspond to overcast skies, and the lower envelope can be attributed to values corresponding to clear skies for a given solar position.

We show the high positive correlation between Q_{pd} and R_d (R^2= 0.997), with a slope of 2.125 ± 0.002 µmol J^{-1} (Figure 11), close to the mean value found for the ratio Q_{pd}/R_d [2.19 ± 0.13 (µmol J^{-1})]. The dependence on sky conditions using the parameters k_t and k_d is shown in Figures 12 and 13. The dispersion of data is high for all sky conditions.

Considering all of the above results, we found it more appropriate to model Q_{pd} rather than Q_{pd}/R_d. Therefore, taking into account our previous model (Foyo-Moreno et al., 2017), the expression of Q_p is:

$$Q_p = a k_t \cos\theta \tag{3}$$

We can separate Q_p into its two components: direct and diffuse. Also, taking into account that global irradiance (R_s) is the sum of the two components (direct and diffuse), we arrive at this expression for Q_{pd}:

$$Q_{pd} = a \cos\theta \frac{R_d}{R_{so}} \tag{4}$$

with a = (2681 ± 2) µmol $m^{-2}s^{-1}$.

3.4. MODEL PERFORMANCE

We have evaluated the model (Eq. 4) at the three stations which were not used in its development. Table 2 shows the results found after including the correlation coefficient R^2 – (the fraction of experimental data variance explained by the model), slope b, and the intercept a of the linear regression of the Q_{pd} measured vs. the estimated values. Table 2 also shows the mean bias error (MBE) and root mean square error (RMSE), both as percentages of the mean experimental values. The MBE and RMSE, are given by the following expressions:

$$MBE = \frac{100}{M_{ave}} \frac{1}{N} \sum_{i=1}^{N} (E_i - M_i) \tag{5}$$

$$RMSE = \frac{100}{M_{ave}} \left(\frac{1}{N} \sum_{i=1}^{N} (E_i - M_i)^2 \right)^{0.5} \tag{6}$$

where E_i is the estimated value (*i*th number), M_i is the measured value, M_{ave} is the average of the measured values and *N* is the number of observations. These two statistics enable the detection both of the differences between experimental data and of the model estimates and the existence of systematic over- or underestimation trends, respectively.

Figure 13 shows Q_{pd} estimated via Eq. (4) at all localities analysed in this work. The model evaluation is excellent for all radiometric stations, the variance explained for the models is better than 95%, and the values for MBE and RMSE vary between -0.3 and 8.6 % and 9.6 and 20.4%, respectively. The model underestimates the values for all localities. In any case, both the slope and correlation coefficient of the linear regression between the measured and estimated values reveals the goodness of the model estimations. Wang et al. (2017), using different soft computing techniques, found MBE values between -16 and -18% and RMSE ranging between 22 and 51% for six stations from the AmeriFlux network.

3. CONCLUSIONS

Two years of measurements made in Granada, an urban site in south-eastern Spain, were used to study the diffuse photosynthetic photon-flux density (Q_{pd}), with the aim of proposing a model for all sky conditions. The model was evaluated at three stations, two in Spain (Granada and Almería) and another in Italy (Renon), with different climatic characteristics. Firstly, we analysed the ratio of Q_{pd} to diffuse irradiance (R_d) to continue with Q_{pd}. The dependence of both (Q_{pd}/R_d and Q_{pd}) on different parameters, which characterize solar position and sky conditions, were considered together with other meteorological factors such as vapour pressure and dewpoint temperature (T_d). The main findings can be summarized as follows:

1. A mean value of 2.19 ± 0.13 µmol J^{-1} was found for Q_{pd}/R_d with values varying between 1.86 and 2.48 µmol J^{-1}.
2. Q_{pd}/R_d showed dependence on parameters that characterize sky conditions such as clearness index (k_t) and diffuse fraction (k_d).
3. A model was proposed to estimate Q_{pd}, taking into account a previous model to estimate the photosynthetic active radiation-flux density (Q_p). This model uses the solar zenith Angle (θ) and R_d as input data.
4. The model provided acceptable results, with a mean bias error varying between -0.3% and 8.8%; and the root mean square error (RMSE) varying between 9.6 and 20.4%.
5. This work suggests that this empirical model can be widely applied from available measurements in most radiometric stations, with better accuracy than other empirical models.

ACKNOWLEDGEMENTS: This work was supported by the Andalusia Regional Government project P12-RNM-2409, by the Spanish Ministry of Economy and Competitiveness projects CGL2013-45410-R and CGL2016-81092-R, and by the European Union's Horizon 2020 research and innovation programme project ACTRIS-2 (grant agreement No 654109). The authors would like to thank the Forestry and Forest Products Research Institute FluxNet Database, FFPRI http://www2.ffpri.affrc.go.jp/labs/flux/).

REFERENCES

Akitsu, T., Nasahara, K.N., Hirose, Y., Ijima, O., Kume, A., 2017. Quantum sensors for accurate and stable long-term photosynthetically active radiation observations. Agric. For. Meteorol. 237-238, 171-183.

Alados, I., Foyo-Moreno, I., Alados-Arboledas, L., 1996. Photosynthetically active radiation: measurements and modeling. Agric. For. Meteorol. 78, 121-131.

Alados, I., Alados-Arboledas L., 1999. Direct and diffuse photosynthetically active radiation: measurements and modelling. Agric. For. Meteorol. 93, 27-38

Alados, I., Olmo, F.J., Foyo-Moreno, I., Alados-Arboledas, L., 2000. Estimation of photosynthetically active radiation under cloudy conditions. Agric. For. Meteorol. 102, 39-50.

Alados, I., Foyo-Moreno, I., Olmo, F.J., Alados-Arboledas, L., 2002. Improved estimation of diffuse photosynthetically active radiation using two spectral models. Agric. For. Meteorol. 101, 1-12.

Batlles, F., Olmo, F., Alados-Arboledas, L., 1995. On shadowband correction methods for diffuse irradiance measurements. Solar Energy 54, 105-114

Dye, D., 2004. Spectral composition and quanta-to-energy ratio of diffuse photosynthetically active radiation under diverse cloud conditions. J. Geophys. Res. 109, D10203 10.1029/2003JD004251

Foyo-Moreno, I., Vida, J., Alados-Arboledas, L., 1998. A simple all weather model to estimate ultraviolet solar radiation (290-385nm). J. Apl. Metereol., 38, 1020–1026.

Foyo-Moreno, I., Alados, I., Olmo, F,J,, Vida, J., Alados-Arboledas, L., 2001. On the use of a cloud modification factor for solar UV (290-385 nm) spectral range. Theor. Appl. Climatol., 68, 41-50.

Foyo-Moreno, I,. Alados, I., Olmo, F.J., Alados-Arboledas, L., 2003. The influence of cloudiness on UV global irradiance (295-385 nm). Agric. For. Meteorol. 120, 101-111.

Foyo-Moreno, I., Alados, I., Alados-Arboledas, L., 2007. Adaptation of an empirical model for erythemal ultraviolet irradiance. Ann. Geophys., 25, 1–10.

Foyo-Moreno, I., Alados, I., Antón, M., Fernández-Gávez, J., Cazorla, A., Alados-Arboledas, L., 2014. Estimating aerosol characteristics from solar irradiance measurements at an urban location in southeastern Spain. J. Geophys. Res. doi: 10.1002/2013JD020599104

Foyo-Moreno, I., Alados, I., Alados-Arboledas, L., 2017. A new conventional regression model to estimate hourly photosynthetic photon flux density under all sky conditions. Int. J. Climatol. doi: 10.1002/joc.5063

Frouin, R., Pinker, R.T., 1995. Estimating photosynthetically active radiation (PAR) at the earth’s surface from satellite observations. Remote Sens Environ 51:98–107

Gu, L., Fuentes, J.D., Shugart, H.H, Staebler, R. M., Black, T.A., 1999. Responses of net ecosystem exchanges of carbon dioxide to changes in cloudiness: Results from two North American deciduous forests. J. Geophys. Res., 104, 31 421–31 434

Gu, L., Baldocchi, D., Verma, S.B., Black, T.A., Vesala, T., Falge, E.M., et al. 2002. Advantages of diffuse radiation for terrestrial ecosystem productivity. J Geophys Res, 107(D6). doi:10.1029/2001JD001242

Gu, L.H., Baldocchi, D.D., Wofsy, S.C., et al., 2003. Response of a deciduous forest to the Mount Pinatubo eruption: Enhanced photosynthesis. Science, 299(5615): 2035–2038.

He, X.Z., Zhou, T., Jia, G.S. et al., 2011. Modeled effects of changes in the amount and diffuse fraction of PAR on forest GPP. Journal of Natural Resources, 26(4): 619–634

Hu, B., Wang, Y., Liu, G., 2007. Spatiotemporal characteristics of photosynthetically active radiation in China. J. Geophys. Res., 112, doi: 10.1029/2006JD007965.

Hu, B., Wang, Y., Liu, G., 2010. Variation characteristics of ultraviolet radiation derived from measurement and reconstruction in Beijing, China, Tellus B 62, 100–108.

Iqbal, M. 1983. An Introduction to Solar Radiation. Academic Press: London.

Jacovides, C.P., Tymvios, F.S., Papaioannou, G., Asimakopoulos, D.N., Theofilou, K.M.,

2004. Ratio of PAR to broadband solar radiation measured in Cyprus, Agric. For. Meteor., 121, 135-140.

Jacovides, C.P., Tymvios, F.S., Asimakopoulos, V.D., Kaltsounides, N.A., 2007. The dependence of global and diffuse PAR radiation components on sky conditions at Athens, Greece, Agric. For. Meteor., 143, 277-287.

Jacovides, C.P., Boland, J., Asimakopoulos, D.N., Kaltsounides, N.A., 2010. Comparing diffuse radiation models with one predictor for partitioning incident PAR radiation into its diffuse component in the eastern Mediterranean basin, Renew. Energy, 35, 1820-1827.

Kanniah, K.D., Beringer, J., North, P., Hutley, L., 2012. Control of atmospheric particles on diffuse radiation and terrestrial plant productivity A review. Progr Phys Geogr , 36(2), 209-237.

Mercado, L.M., Bellouin, N., Sitch, S. et al., 2009. Impact of changes in diffuse radiation on the global land carbon sink. Nature, 458(7241): 1014–1017.

Min, Q., 2005. Impacts of aerosols and clouds on forest-atmosphere carbon exchange. J Geophys Res110:D066203. doi:10.1029/2004JD004858.

Misson, L., Lunden, M., McKay, M., Goldstein, A.H., 2005. Atmospheric aerosol light scattering and surface wetness influences the diurnal pattern of net ecosystem exchange in a semi-arid ponderosa pine plantation. Agric For Meteorol 129:60–83.

Perez, R., Ineichen, P., Seals, R., Michalsky, J.J., Stewart, R., 1990. Modelling daylight availability and irradiance components from direct and global irradiance. Solar Energy 44, 271-289.

Reitan, C.H., 1963. Surface dewpoint and water vapour aloft. J. Appl. Meteorol., 2: 776-779.

Singh, J., Bhattacharya, B.K., Kumar, M., Mallick, K.. 2013. Modelling monthly diffuse solar radiation fraction and its validity over the Indian sub-tropics. Int. J. Climatol., 33, 77-

86.
Spitters, C.J.T., Toussaint, H.A.J.M., Goudriaan, J. 1986. Separating the diffuse and direct component of global radiation and its implications for modelling canopy photosynthesis. Agric For Meteorol, 38:217–29
Sun, J.S., Zhou, G.S., 2010. Review of advances in measurements and effects of diffuse radiation on terrestrial ecosystem productivity. Chinese Journal of Plant Ecology, 34(4): 452–461. (in Chinese).
Tang, W., Qin, J., Yang, K., Niu, X., Zhang, X., 2013. Reconstruction of daily photosynthetically active radiation and its trend over China.J. Geophys. Res. Atm., 118, 13292-13302.
Udo, S., Aro, T., 1999. Global PAR related to global solar radiation for central Nigeria. Agric. For. Meteorol. 97, 21–31, http://dx.doi.org/10.1016/S0168-1923(99)55-6.
Wang, L., Gong, W., Ma, Y., Hu, B., Zhang, M., 2014. Photosynthetically active radiation and its relationship with global solar radiation in Central China. Int. J. Biometorol., 58, 1265-1277.
Wang, L., Hu, B., Kisi, O., Zounemat-Kermani, M., Gong, W., 2017. Prediction of diffuse photosynthetically active radiation using different soft computing tcheniques. Q. J. R. Meteorol. Soc., doi: 10.1002/qj.3081.
Yu, X., Wu, Z., Jiang, W., Guo, X., 2015. Predicting daily photosynthetically active radiation from global solar radiation in the Contiguous United States. Energy Convers. Manage., 89, 71-82.
Yu, X., Guo, X., 2016. Hourly photosynthetically active radiation estimation in Midwestern United States from artificial neural networks and conventional reression models. Int. J. Biometorol., 60, 1247-1259.

Zhang, M., Yu, G.R., Zhang, L.M. et al., 2010. Impact of cloudiness on net ecosystem exchange of carbon dioxide in different types of forest ecosystems in China. Biogeosciences, 7(2): 711–722.

Zhang, M., Yu, G.R., Zhuang, J. et al., 2011. Effects of cloudiness change on net ecosystem exchange, light use efficiency, and water use efficiency in typical ecosystems of China. Agric.For.Meteorol.151(7),803–816.

Sites	T (ºC)	TM (ºC)	Tm (ºC)	R (mm)	U (%)
Granada, Spain (37.16° N, 3.6º W, 650 m a.s.l.)	15.4	23.0	7.8	365	58
Almería, Spain (36.83° N, 2.41º W, 21 m a.s.l)	19.1	23.4	14.7	200	65
Renon, Italy (46.42° N, 11.28° E,1735 m a.s.l)	4.1	18.0	5.2	1010	

Table 1: Description and climatic data of study sites. T (yearly average temperature), TM (yearly average of the maximum temperature), Tm (yearly average of the minimum temperature), R (yearly average of precipitation), U (yearly average of relative humidity).

Sites	Years	N	kt	k	$Q_{pd,ave}$ (μmol $m^{-2}s^{-1}$)	a (μmol $m^{-2}s^{-1}$)	b	R_2	MBE (%)	RMSE (%)
Granada	94-95	3448	0.54±0.19	0.55±0.30	428	-30.8 ± 0.8	0.992 ± 0.002	0.99	-7.7	9.6
Almeria	93-95	5797	0.58±0.18	0.50±0.30	419	-19.5 ± 1.1	0.959 ± 0.002	0.96	-8.8	12.9
Renon	13-15	16980	0.45 ±0.27	0.59±0.35	296	-60.3 ±0.7	1.200±0.002	0.95	-0.3	20.4

Table 2: Statistical results of the new empirical model to estimate Q_{pd} at each station. N (total number of observations). $Q_{pd,ave}$ (average values of Q_{pd}). Linear regression statistics: a (intercept), b (slope) and R^2 (correlation coefficient). MBE (Mean Bias Error). RMSE (Root Mean Square Error).

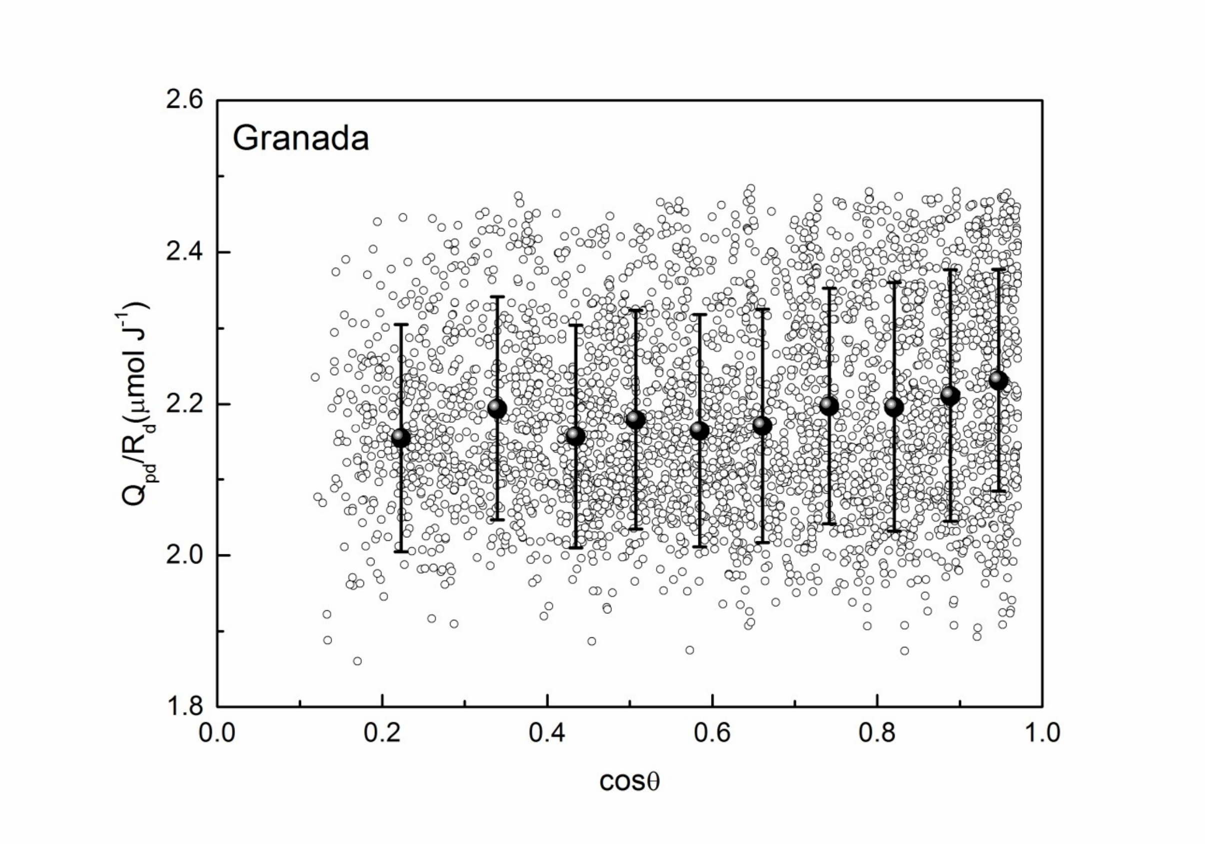

Figure 1: Ratio of diffuse photosynthetic photon flux density to diffuse irradiance (Q_{pd}/R_d) vs. the cosine of solar zenith angle (cos θ). Small dots denote experimental data, black symbols represent mean values, and bars denote standard deviations for each of the intervals in cos θ.

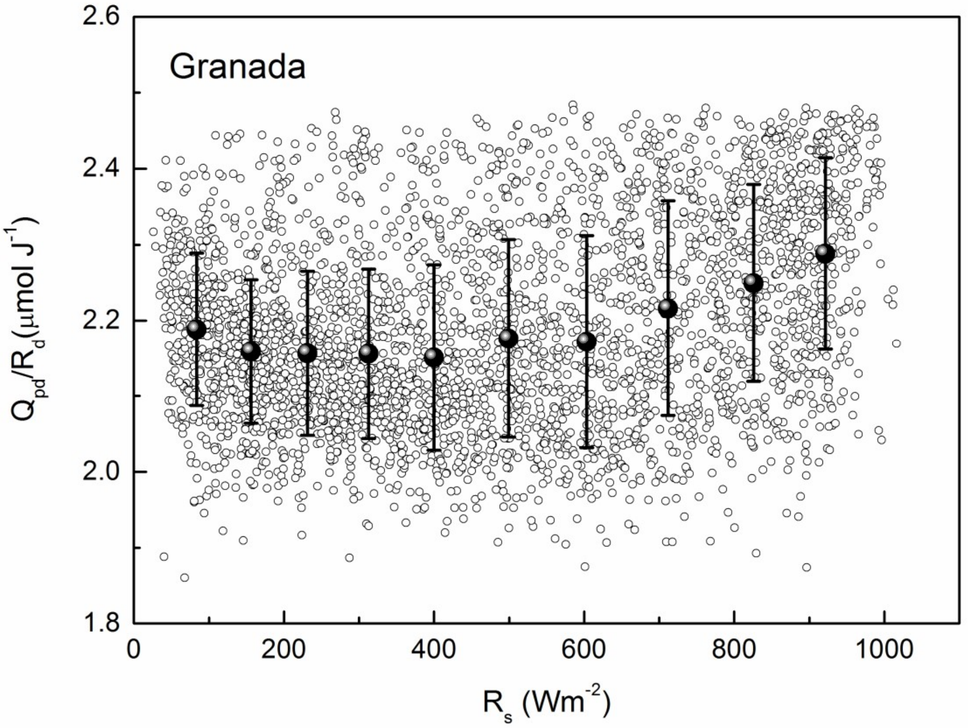

Figure 2: Ratio of diffuse photosynthetic photon flux density to diffuse irradiance (Q_{pd}/R_d) vs. broadband solar irradiance (R_s). Small dots denote experimental data, black symbols represent mean values, and bars denote standard deviations for each of the intervals in R_s.

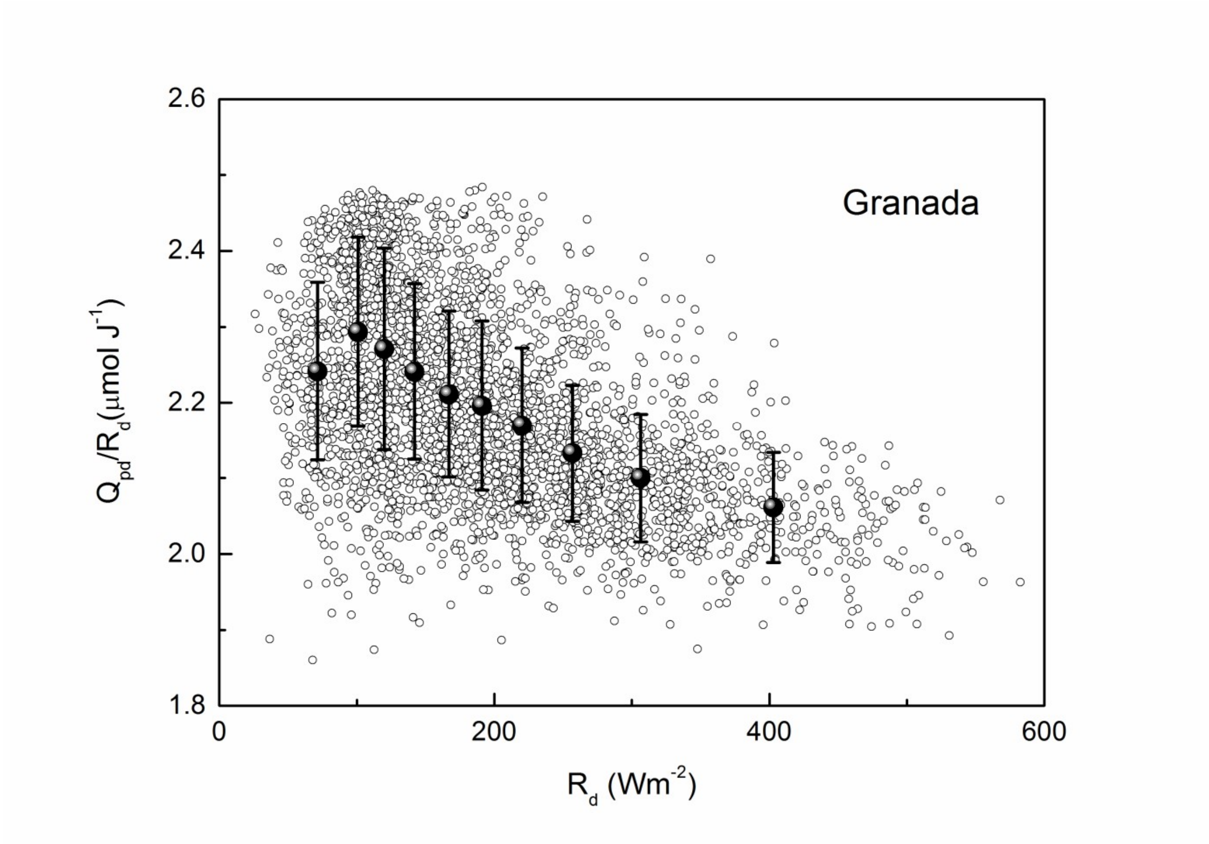

Figure 3: Ratio of diffuse photosynthetic photon flux density to diffuse irradiance (Q_{pd}/R_d) vs. diffuse irradiance (R_d). Small dots denote experimental data, black symbols represent mean values, and bars denote standard deviations for each of the intervals in R_d.

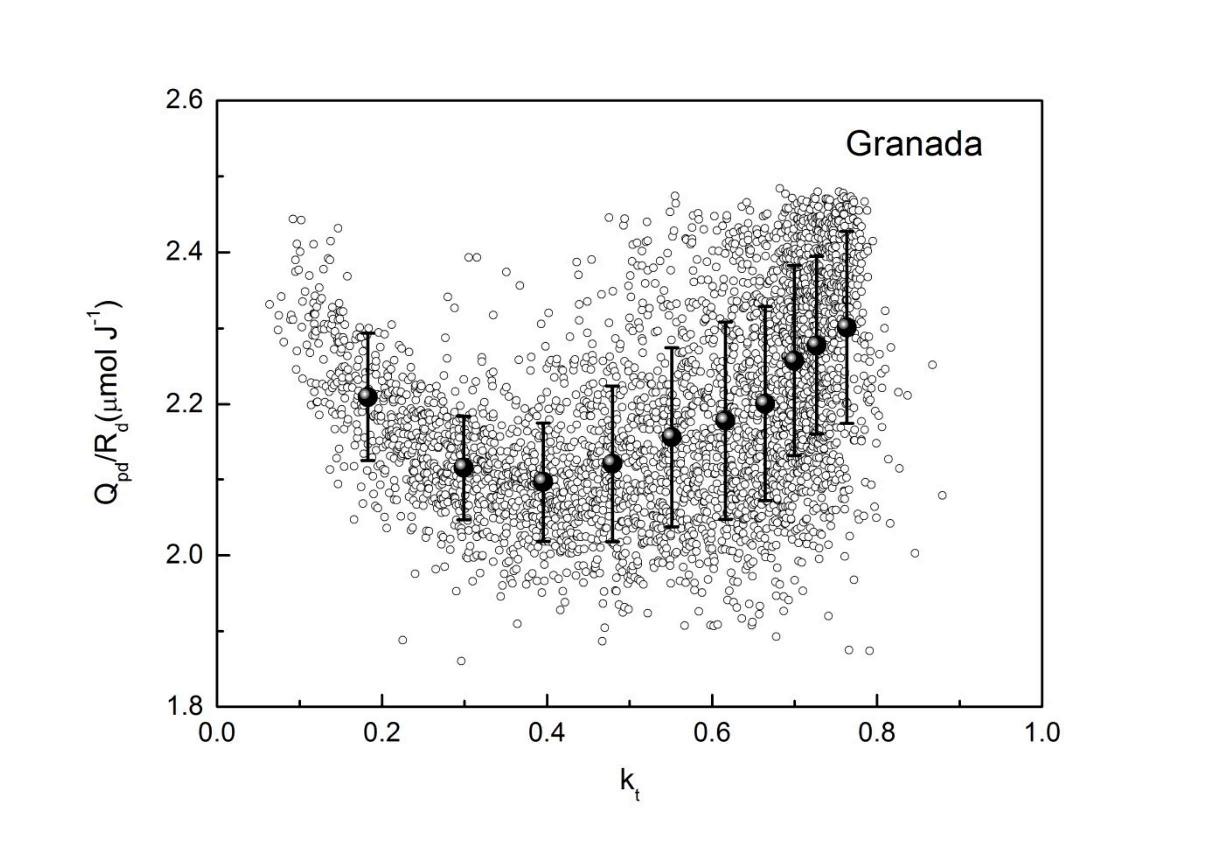

Figure 4: Ratio of diffuse photosynthetic photon flux density to diffuse irradiance (Q_{pd}/R_d) vs. clearness index (k_t). Small dots denote experimental data, black symbols represent mean values, and bars denote standard deviations for each of the intervals in k_t.

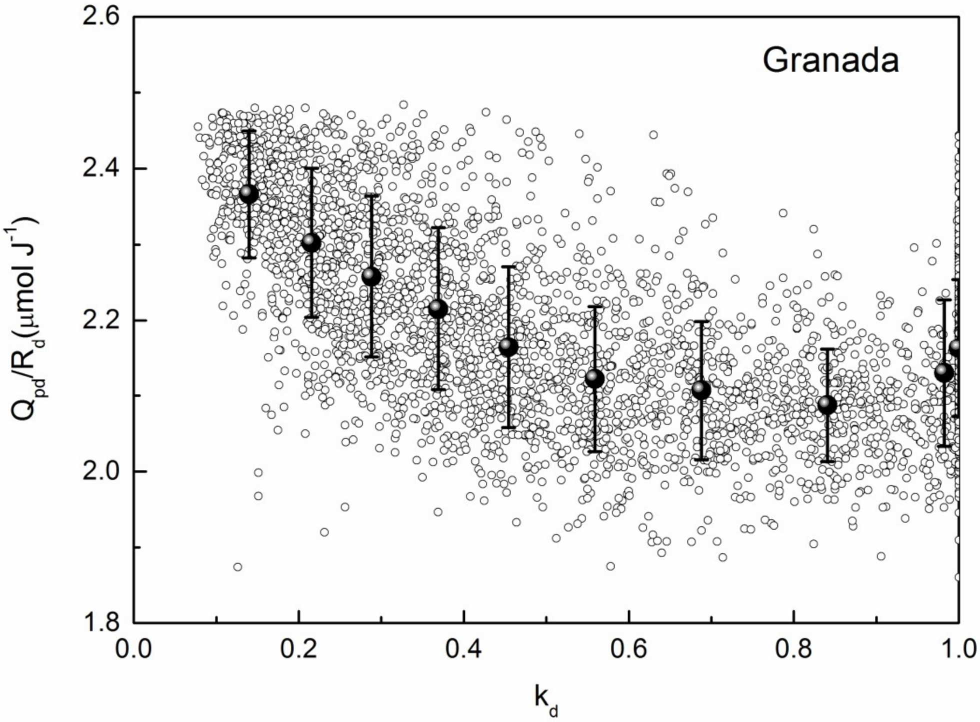

Figure 5: Ratio of diffuse photosynthetic photon flux density to diffuse irradiance (Q_{pd}/R_d) vs. k_d. Small dots denote experimental data, black symbols represent mean values and bars denote standard deviations for each of the intervals in k_d.

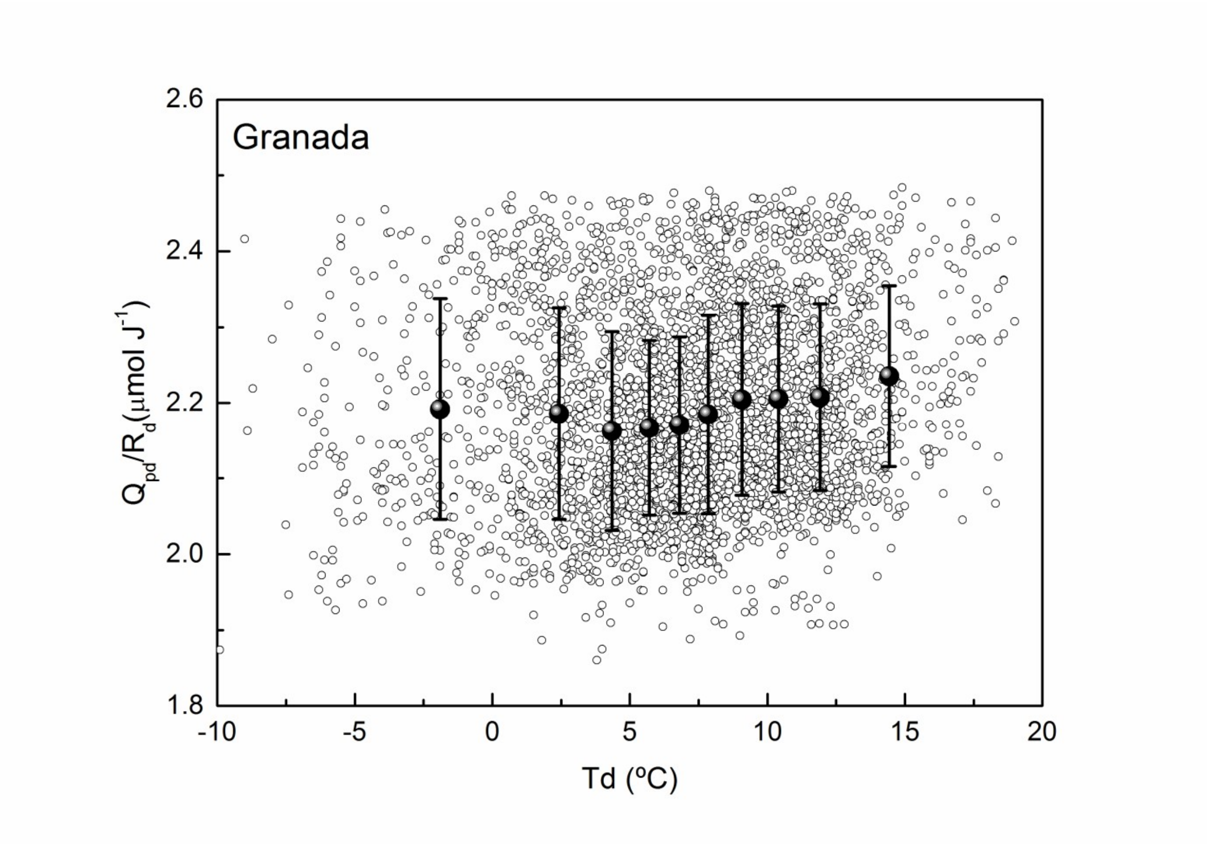

Figure 6: Ratio of diffuse photosynthetic photon flux density to diffuse irradiance (Q_{pd}/R_d) vs. the dewpoint temperature (T_d). Small dots denote experimental data, black symbols represent mean values, and bars denote standard deviations for each of the intervals in T_d.

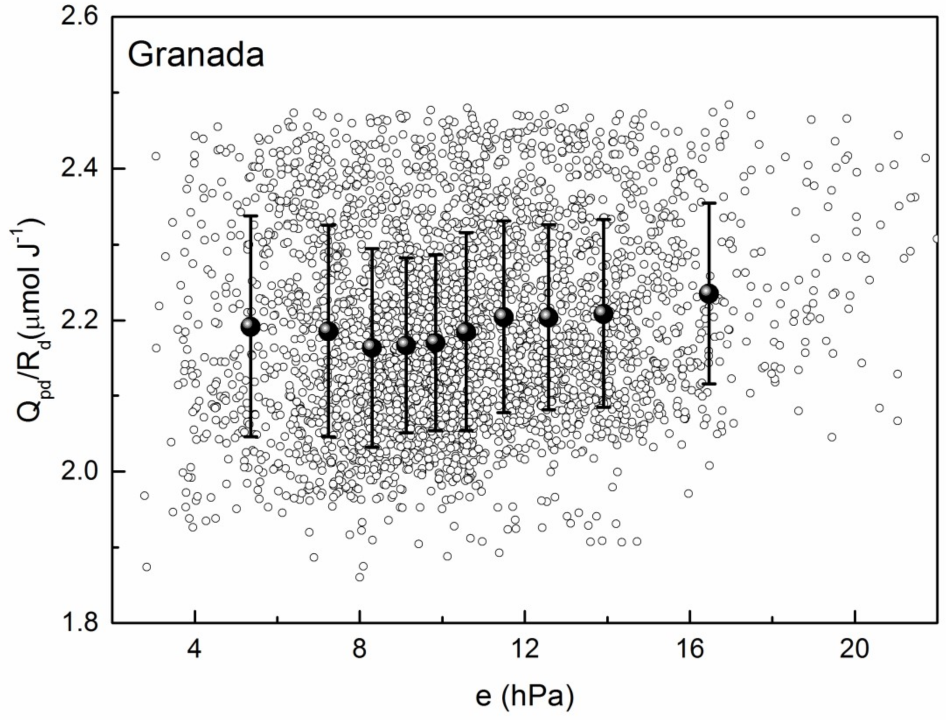

Figure 7: Ratio of diffuse photosynthetic photon flux density to diffuse irradiance (Q_{pd}/R_d) vs. the partial vapour pressure (e). Small dots denote experimental data, black symbols represent mean values, and bars denote standard deviations for each of the intervals in e.

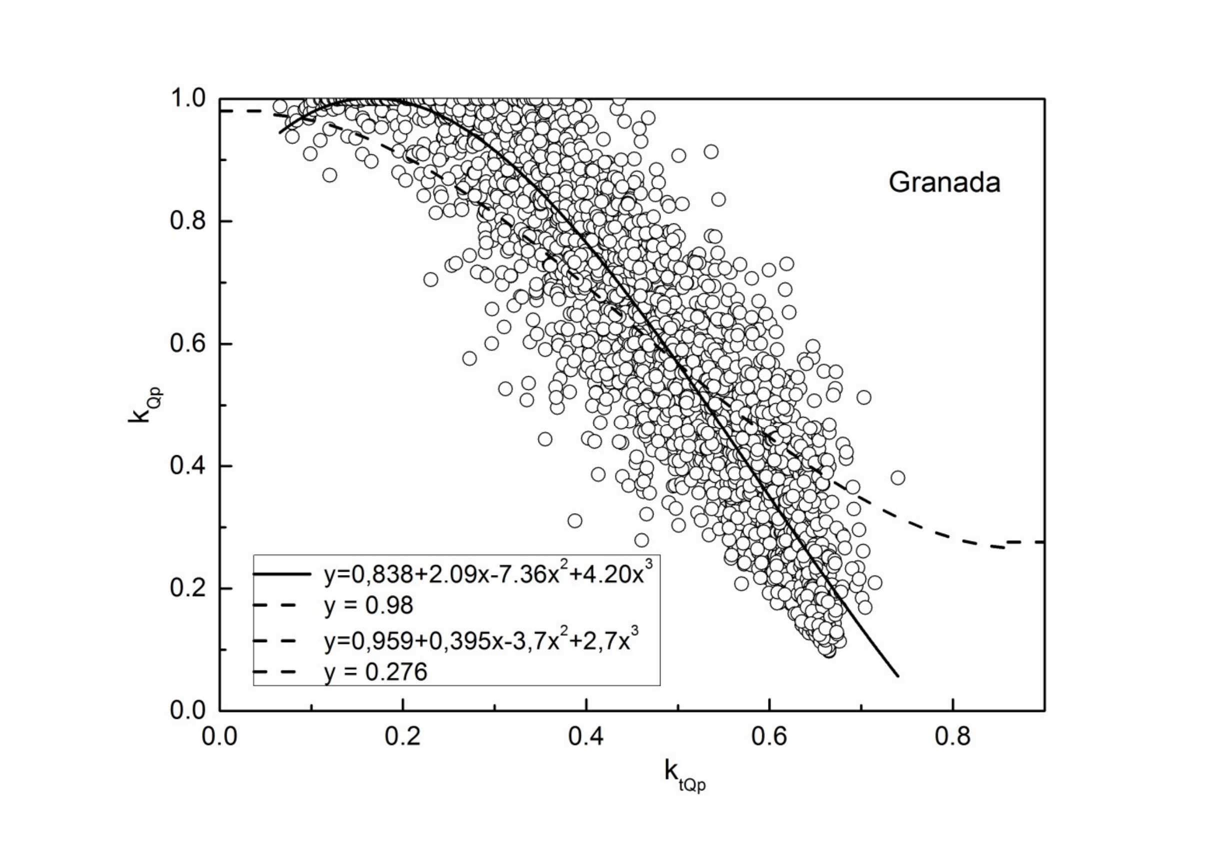

Figure 8: Diffuse fraction in the visible range (k_{dQp}) vs. clearness index in the visible range (k_{tQp}). Small dots denote experimental data. Dashed lines denote polynomial fitting (Jacovides et al. 2007). Solid lines denote our polynomial fitting.

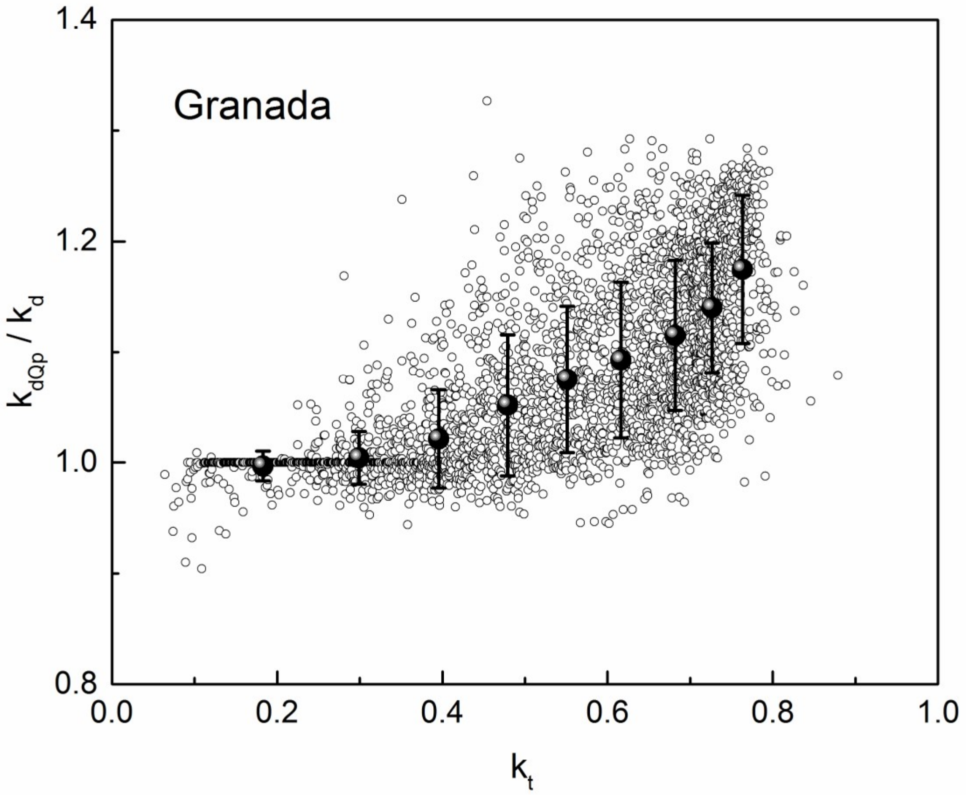

Figure 9: Ratio of diffuse fraction in the visible range (k_{dQp}) and diffuse fraction in the shortwave broadband range (k_d) vs. clearness index (k_t). Small dots denote experimental data, black symbols represent mean values, and bars denote standard deviations for each of the interval in k_t.

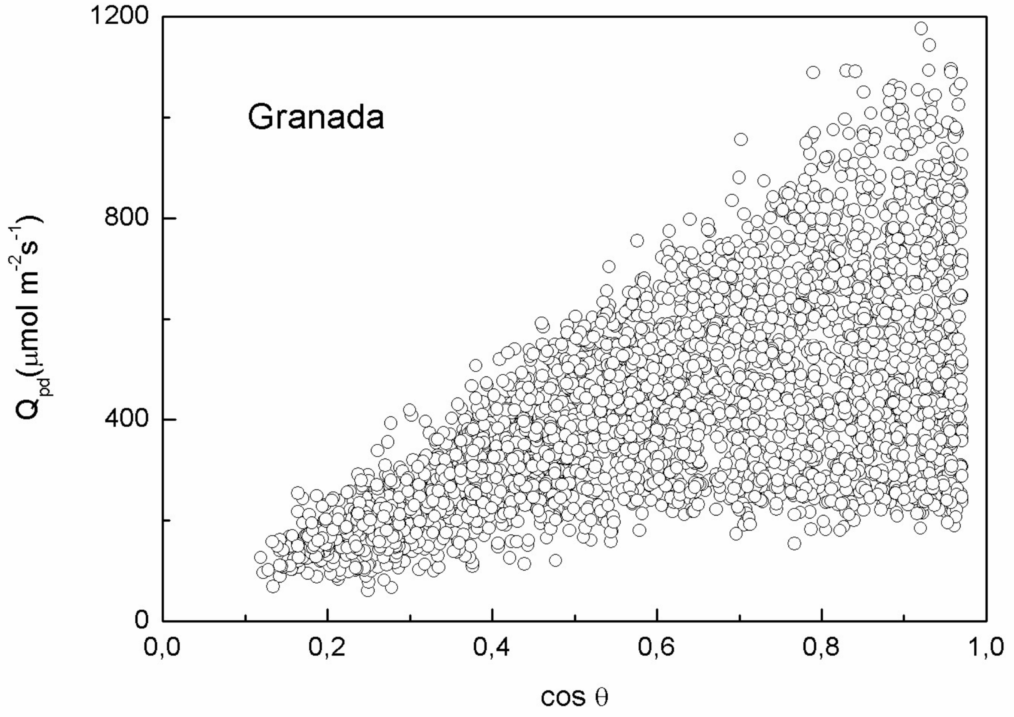

Figure 10: Diffuse photosynthetic photon flux density (Q_{pd}) vs. cosine of the solar zenith angle (cos θ). Dots represent experimental data.

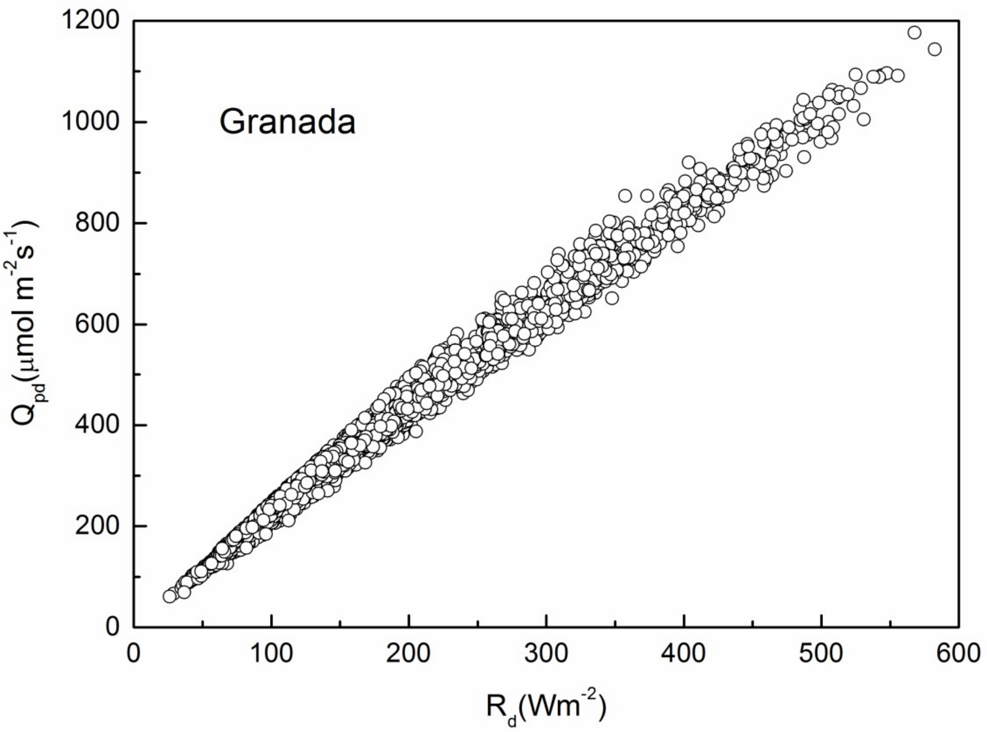

Figure 11: Diffuse photosynthetic photon flux density (Q_{pd}) vs. R_d. Dots represent experimental data.

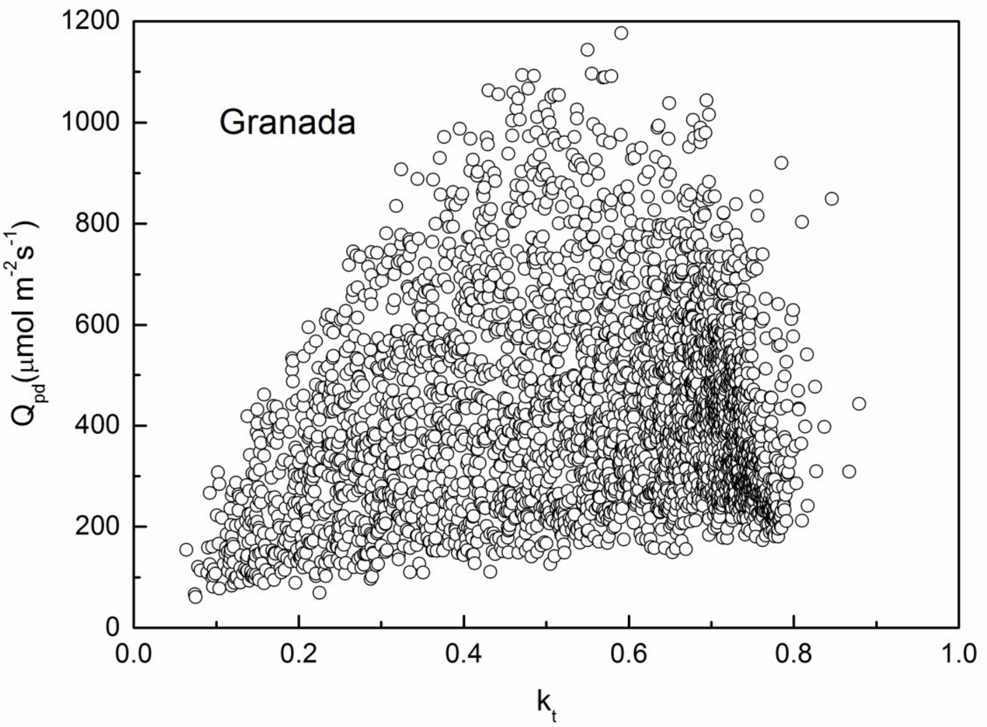

Figure 12: Diffuse photosynthetic photon flux density (Q_{pd}) vs. k_t. Dots represent experimental data.

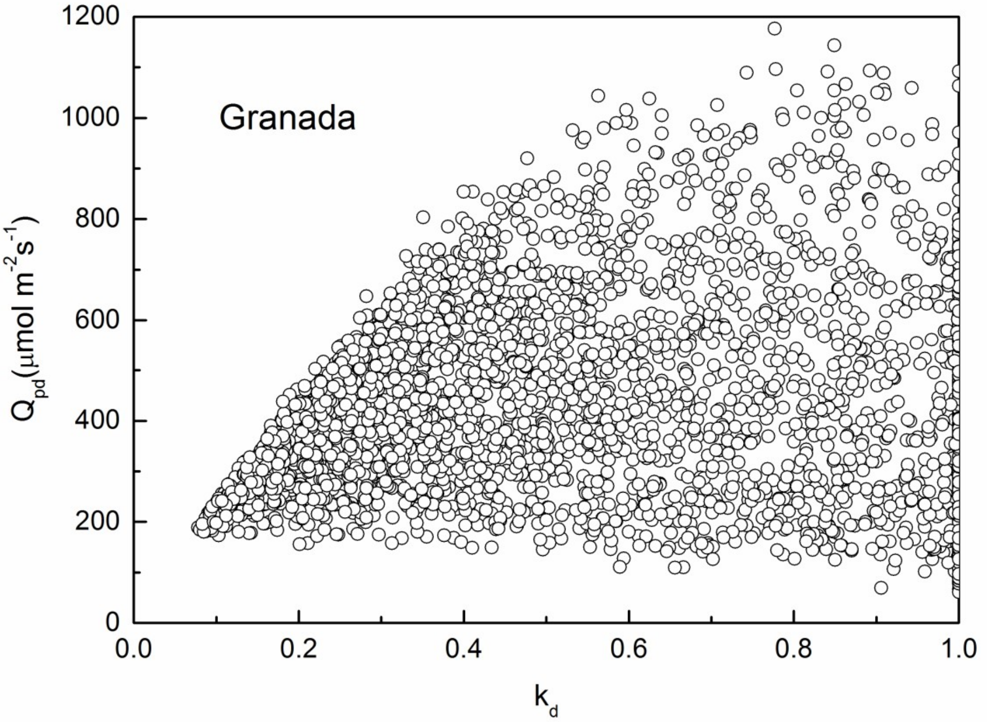

Figure 13: Diffuse photosynthetic photon flux density (Q_{pd}) vs. k_d. Dots represent experimental data.

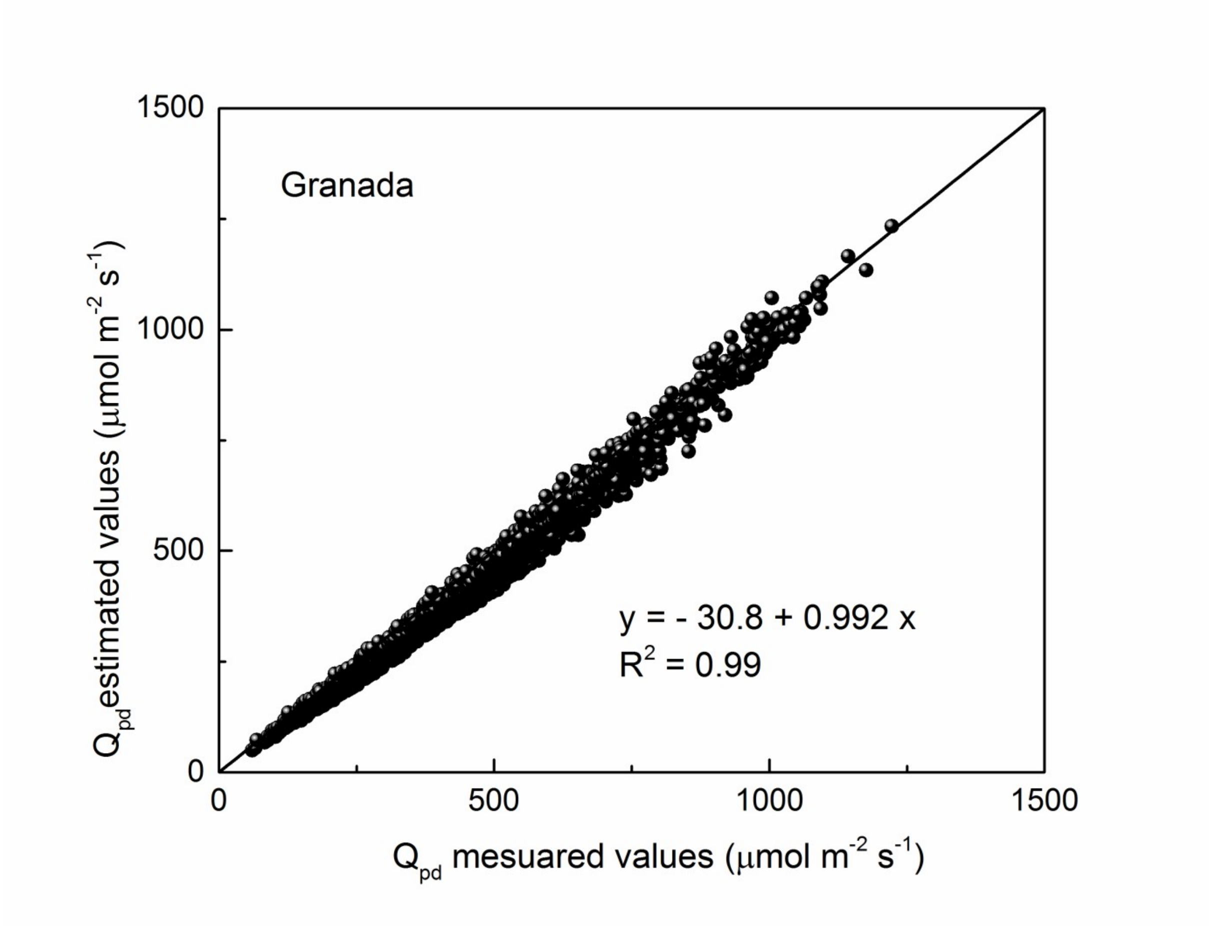

Figure 14 a: Scatter plot of estimated vs. measured values of photosynthetic photon flux density (Q_{pd}) at Granada site.

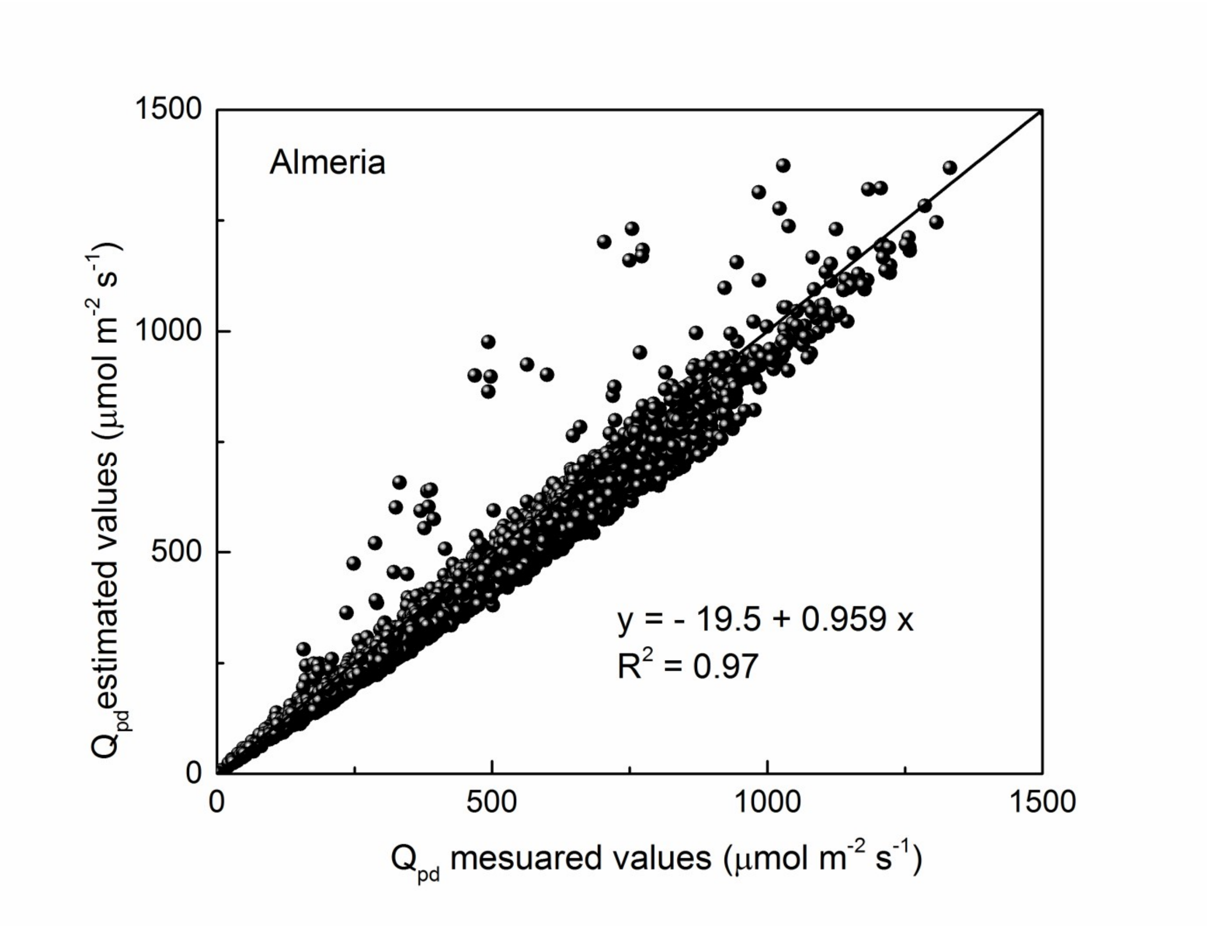

Figure 14 b: Scatter plot of estimated vs. measured values of photosynthetic photon flux density (Q_{pd}) at Almeria site.

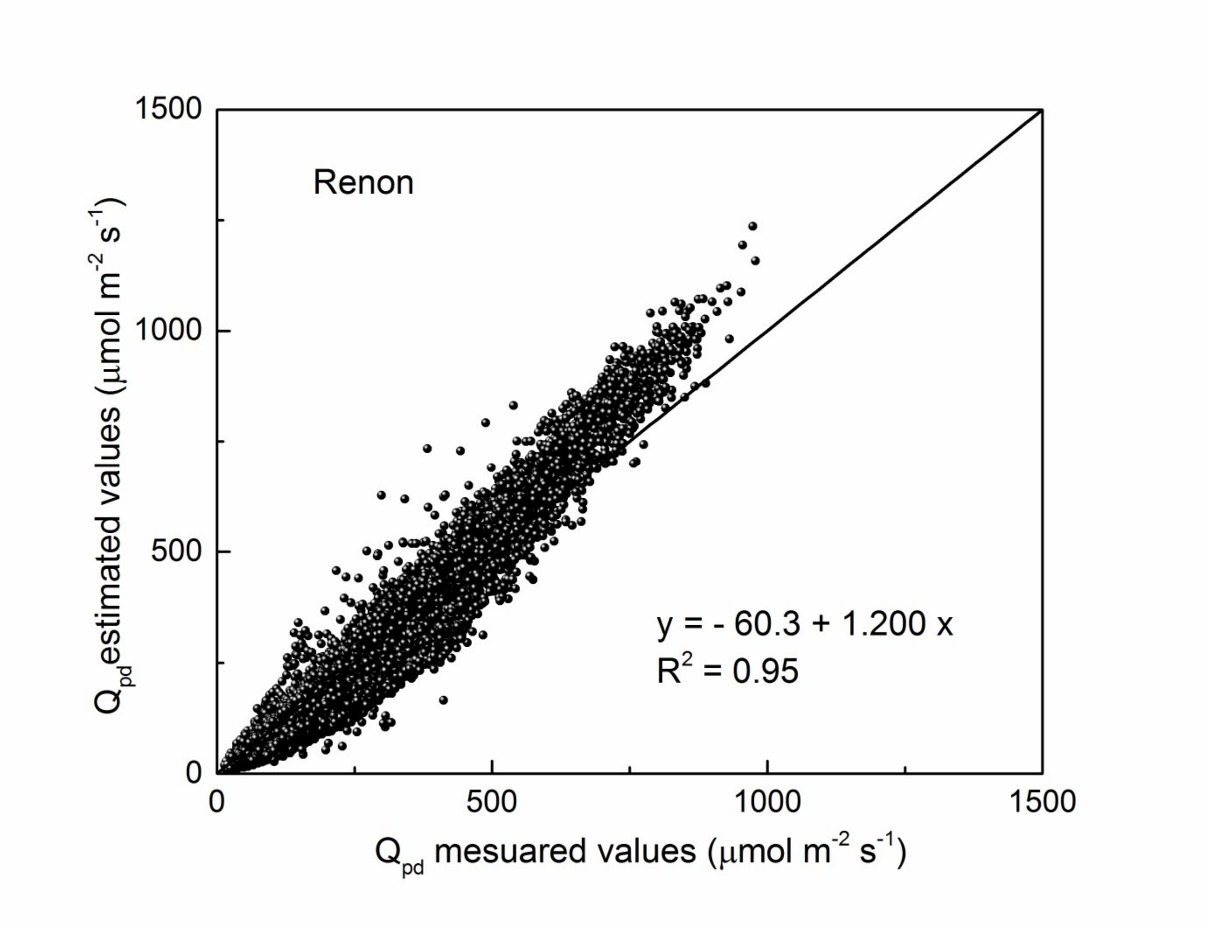

Figure 14c: Scatter plot of estimated vs. measured values of photosynthetic photon flux density (Q_{pd}) at Renon site.